Does Changing the Predicted Dynamics of a Phospholipase C Alter Activity and Membrane Binding?

Jiongjia Cheng,[†] Sashank Karri,[‡] Cédric Grauffel,[§] Fang Wang,[¶] Nathalie Reuter,[§] Mary F. Roberts,[†] Patrick L. Wintrode,[¶] and Anne Gershenson[||*]

[†]Department of Chemistry, Boston College, Chestnut Hill, Massachusetts; [‡]Department of Biophysics & Physiology, Case Western Reserve University School of Medicine, Cleveland, Ohio; [§]Department of Molecular Biology, University of Bergen, Bergen, Norway; [¶]Department of Pharmaceutical Sciences, University of Maryland School of Pharmacy, Baltimore, Maryland; and [||]Department of Biochemistry & Molecular Biology, University of Massachusetts, Amherst, Massachusetts

ABSTRACT The enzymatic activity of secreted phosphatidylinositol-specific phospholipase C (PI-PLC) enzymes is associated with bacterial virulence. Although the PI-PLC active site has no obvious lid, molecular-dynamics simulations suggest that correlated loop motions may limit access to the active site, and two Pro residues, Pro^{245} and Pro^{254}, are associated with these correlated motions. Whereas the region containing both Pro residues is quite variable among PI-PLCs, it shows high conservation in virulence-associated, secreted PI-PLCs that bind to the surface of cells. These regions of the protein are also associated with phosphatidylcholine binding, which enhances PI-PLC activity. In silico mutagenesis of Pro^{245} disrupts correlated motions between the two halves of *Bacillus thuringiensis* PI-PLC, and Pro^{245} variants show significantly reduced enzymatic activity in all assay systems. PC still enhanced activity, but not to the level of wild-type enzyme. Mutagenesis of Pro^{254} appears to stiffen the PI-PLC structure, but experimental mutations had minor effects on activity and membrane binding. With the exception of P245Y, reduced activity was not associated with reduced membrane affinity. This combination of simulations and experiments suggests that correlated motions between the two halves of PI-PLC may be more important for enzymatic activity than for vesicle binding.

INTRODUCTION

Phosphatidylinositol-specific phospholipase C (PI-PLC) enzymes are virulence factors for both extracellular (1) and intracellular bacterial pathogens including *Bacillus anthracis* (2) and *Listeria monocytogenes* (3), respectively. In contrast to their multidomain eukaryotic relatives, these bacterial PI-PLCs contain only the monomeric catalytic domain that is responsible for both catalysis and membrane binding. Although PI-PLC catalytic domains are members of the triosephosphate isomerase (TIM) barrel $(\alpha/\beta)_8$ superfamily (4–6) they lack a number of hydrogen-bonding interactions between β-strands 5 and 6, resulting in a relatively open β-barrel (4,5) (Fig. 1 *A*). The conserved active site is located at the C-terminal end of the β-strands in the barrel (4,5), but most of the residues that interact with membranes and control lipid binding in the bacterial enzymes are located in the less conserved and more mobile surface helices and loops.

Bacillus PI-PLCs can cleave phosphatidylinositol (PI) in a large variety of contexts. Physiologically, they cleave glycosylphosphatidylinositol-anchored proteins on the outer leaflet of eukaryotic cell plasma membranes contributing to bacterial virulence (7–9). In vitro, these PI-PLCs catalyze the hydrolysis of PI to yield diacylglycerol (DAG) and 1,2-cyclic inositol phosphate (cIP), and further hydrolyze soluble cIP to myo-inositol 1-phosphate (I-1-P) (Scheme 1) (4,10). These activities are specifically enhanced by two phospholipids that are commonly found in the outer membranes of eukaryotic cells, phosphatidylcholine (PC) and sphingomyelin (11–13). Activity enhancement is associated with increased affinity for surfaces containing even small amounts of PC (14,15) and decreased dynamics of the phospholipid headgroups (14), but the role of protein dynamics in binding and activity is still unclear.

To investigate the importance of PI-PLC dynamics in membrane binding and enzymatic activity, molecular dynamics (MD) simulations were performed starting from the x-ray crystal structure of free *Bacillus cereus* PI-PLC (4). The MD simulations for *Bacillus* PI-PLC showed anticorrelated motions between the first two-thirds and last one-third of the PI-PLC structure, essentially the two halves of the β-barrel. Such anticorrelated barrel motions were not observed in MD simulations for the intracellular bacterial pathogen *L. monocytogenes* PI-PLC. In addition, *Bacillus* PI-PLC showed coordinated motion closing of loops over the active site. Multiple sequence alignments (MSAs) revealed that a number of residues in these loops are conserved in *Bacillus, Staphylococcus*, and other extracellular bacterial pathogens, but not in *Listeria*.

Both the MD simulations and conservation results suggested that Pro residues 245 and 254 in helix G of *Bacillus* PI-PLC might be important for the correlated motions. Mutagenesis of Pro^{245}, the residue that caps helix G, disrupted the correlated motion of the barrel seen in the PI-PLC MD simulations and greatly reduced enzymatic activity.

Submitted July 9, 2012, and accepted for publication November 19, 2012.

*Correspondence: gershenson@biochem.umass.edu

Sashank Karri's current address is Mount Sinai School of Medicine, New York, NY.

Editor: Bert de Groot.

0006-3495/13/01/0185/11 $2.00

http://dx.doi.org/10.1016/j.bpj.2012.11.015

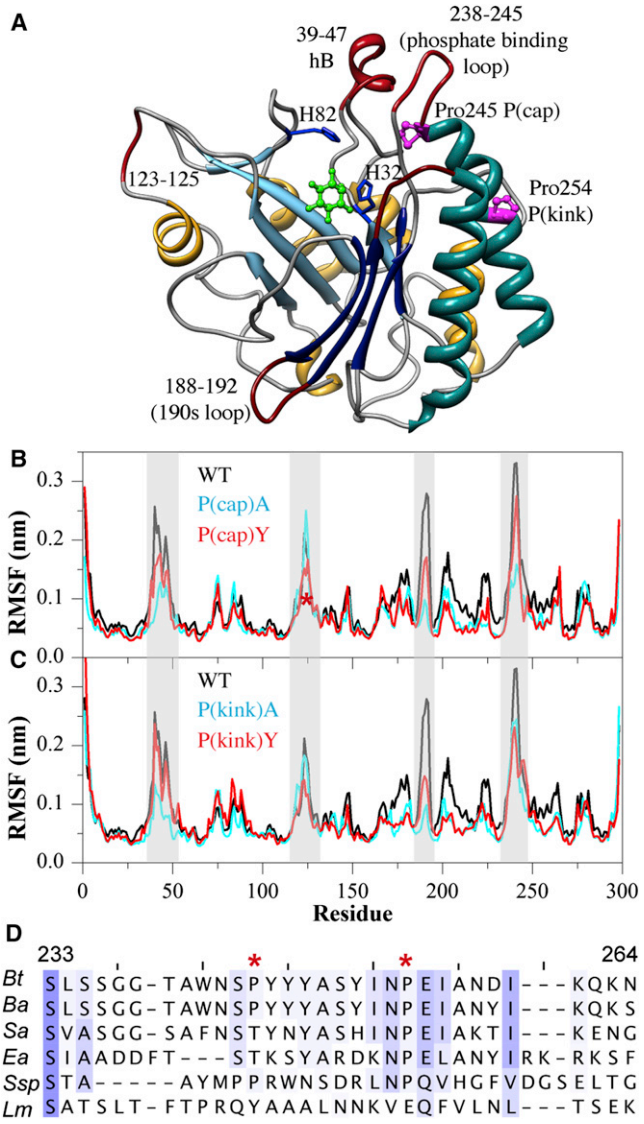

FIGURE 1 Structure, dynamics, and conservation of *Bacillus* PI-PLC. (*A*) The x-ray crystal structure of *B. cereus* PI-PLC (PDB:1PTG (4)) made using UCSF Chimera (64) showing the N-terminal and C-terminal halves of the β-barrel (*light blue* and *dark blue*, respectively), helices F and G (*turquoise*), regions that show large fluctuations in the WT MD simulations (*dark red*) and the active site indicated by His residues 32 and 82 (*blue*) and myo-inositol (*green*). The two Pro residues of interest are also shown (*pink*). RMSFs from the MD simulations in solution for (*B*) P(cap) variants and (*C*) P(kink) variants with WT (*black*), Pro to Ala variants (*cyan*), and Pro to Tyr variants (*red*). Regions with the largest fluctuations are highlighted (*gray*). (*D*) A selection from the multiple sequence alignment clustered using the helix G region from JALVIEW (35) with Blosum62-based coloring. Higher conservation is also depicted (*darker shading*). The abbreviations are: Bt, *Bacillus thuringiensis*; Ba, *Bacillus anthracis*; Sa, *Staphylococcus aureus*; Ea, *Erwinia amylovora* (fireblight); Ssp, *Streptomyces* species; Lm, *Listeria monocytogenes*.

Some Pro^{245} variants also had significantly reduced affinity for membranes. Pro^{254} in helix G is associated with a kink in helix G. In silico mutagenesis of Pro^{254} to Ala or Tyr damped loop and helix motions, and enzymatic activity of purified Pro^{254} variants was affected in some assay systems, notably those lacking phosphatidylcholine (PC), an activating lipid for this enzyme (11–13). However, the binding affinities were similar to wild-type (WT). Further tests of the role of dynamics in PI-PLC activity were performed by altering the flexibility of the 190s loop. This loop is far from the active site- and membrane-binding regions of PI-PLC, but the simulations suggested that it plays a role in PI-PLC clamshell motions. Mutations in the 190s loop aimed at altering loop flexibility significantly decreased activity in the absence of PC, suggesting that dynamics in this hitherto ignored part of the enzyme may be important. Taken together, these results suggest that correlated motions in PI-PLC, involving loops and helices that can close over the active site, may be important factors in optimizing enzymatic activity, particularly in the absence of PC, for PI-PLCs from extracellular bacterial pathogens.

MATERIALS AND METHODS

MD simulations and analysis

Simulations in solution

MD simulations for *Bacillus* PI-PLC were conducted with the software NAMD Ver. 2.7 (16), utilizing the CHARMM force field (17) with the CMAP correction (18,19) and TIP3P water (20). Simulations were performed using particle-mesh Ewald electrostatics and periodic boundary conditions. The crystal structure for *B. cereus* PI-PLC (PDB:1PTG (4)) was used as a starting point with the missing C-terminal two amino acids, Lys^{297} and Glu^{298}, modeled into the structure. Simulations were carried out in the NPT ensemble. Ionizable residues were in their standard protonation states at pH 7. Protonation states of histidine residues were assigned using the software package PROPKA (21). The solvated, energy minimized system was heated to 310 K in 10° steps, and simulations were run for 20 ns with the last 15 ns used for analysis. Four simulations in total were performed for wild-type PI-PLC, with two simulations run for each Pro variant. *B. cereus* and *Bacillus thuringiensis* PI-PLC sequences are 97% identical, and a single MD simulation using the *B. thuringiensis* sequence was not significantly different. Principal component analyses (PCA) were performed using the program WORDOM (22). An MD simulation for *L. monocytogenes* PI-PLC was downloaded from the molecular-dynamics database MoDEL (23) and analyzed using WORDOM (22). Cross-correlation and chained-correlation analyses were carried out using the FlexServe webserver (24). Chained correlations were used to identify residues in potential long-range communication by calculating intermediate correlations (25). For this calculation, a root residue is chosen and the w most highly correlated residues above a chosen cutoff are selected. Each of these residues is then taken as a root for another iteration, and this procedure is repeated for D iterations, with $w = 3$, $D = 5$, and a cutoff of 0.5.

Simulations with membranes

MD simulations with an explicit, flat bilayer containing 256 dimyristoylphosphatidylcholine (DMPC) lipids and two copies of *B. cereus* PI-PLC (PDB:1PTG (4)), one on each side of the bilayer using the x-ray crystal structure as the initial conformation, were performed using the CHARMM36 force field (26). The initial orientation of PI-PLC relative to the bilayer was determined from simulations using an implicit IMM1-GC membrane model (27) as previously described in Hajjar et al. (28). The total simulation time was 50 ns and, for each copy of the protein, the last 20 ns were analyzed as described above. The DMPC bilayer was taken from Broemstrup and Reuter (29) and further equilibrated for 20 ns with the

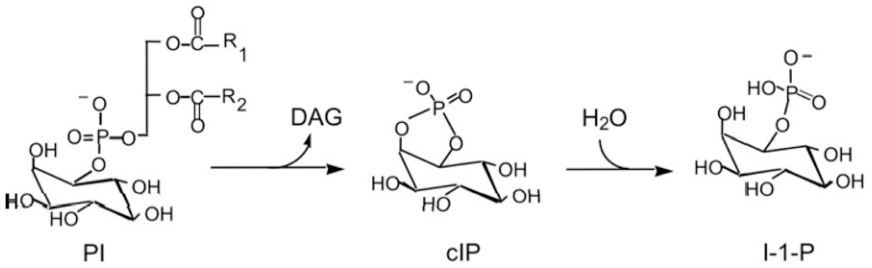

SCHEME 1 The two sequential reactions catalyzed by *Bacillus* PI-PLC.

CHARMM36 force field (the average surface area per lipid was 60.1 ± 0.8 Å^2). Four lipids on each side of the bilayer were removed to reduce steric clashes. The system was then solvated by TIP3P water molecules (80 × 80 × 170 Å^3) (20) and 12 sodium ions were added to attain an electrostatically neutral system. Using this protocol, we built two systems that differ only by an offset in the position of the proteins (to avoid bias due to initial protein-lipid interactions). Simulations were performed using NAMD (16) with further details provided in the Supporting Material. Backbone root-mean-square deviations compared to the minimized x-ray crystal structure were monitored and reveal an overall stable PI-PLC structure (see Fig. S1 in the Supporting Material). Analyses presented here were performed on the last 20 ns of the 50-ns simulations.

Multiple sequence alignments

Multiple sequence alignments (MSAs) were performed on the National Center for Biotechnology Information website using three rounds of the algorithms PSI-BLAST (30) and COBALT (31). After the first and second rounds, the PSI-BLAST results were manually pruned to remove redundant sequences. Sequence alignments based on BLAST rather than PSI-BLAST results were not significantly different. Sequence similarity based on comparisons between all sequence pairs in the alignment using either the full protein sequences or parts of the *B. thuringiensis* protein sequence were determined as previously described in Marcelino et al. (32). The resulting two-dimensional matrix was clustered using a city block distance matrix and the program CLUSTER 3.0 (33) and the results were displayed using the softwares TREEVIEW (34) and JALVIEW (35).

Reagents

L-α-phosphatidylinositol (PI) and other phospholipids, including short-chain lipid diheptanoyl-PC (diC$_7$PC), and long-chain lipids 1-palmitoyl-2-oleoylphosphatidylcholine (POPC) and 1,2-dioleoyl-*sn*-glycero-3-phospho-(1′-rac-glycerol) (DOPG), were purchased from Avanti Polar Lipids (Alabaster, AL) and used without further purification. cIP was produced from crude soybean PI (Sigma-Aldrich, St. Louis, MO) as described previously in Zhou et al. (13). All competent cells used in mutagenesis (XL1-Blue) and overexpression (BL21 Codonplus) were obtained from Agilent (Santa Clara, CA). The fluorophore Alexa Fluor 488 C$_5$ maleimide (AF488) was purchased from Invitrogen (now Life Technologies, Grand Island, NY). Q-sepharose fast-flow anion-exchange resin and phenyl-sepharose hydrophobic resin were purchased from GE Healthcare (Piscataway, NJ) and Sigma-Aldrich, respectively. Bio-Spin 6 columns were obtained from Bio-Rad (Hercules, CA).

Purification, secondary structure, and thermostability

The wild-type (WT) *B. thuringiensis* PI-PLC gene was mutated as previously reported in the literature (36–38), using the QuikChange Mutagenesis Kit (Stratagene, La Jolla, CA) with primers from Operon (Huntsville, AL). All mutations were confirmed by DNA sequencing (Genewiz, South Plainfield, NJ). Plasmids containing the various PI-PLC genes were transformed into *Escherichia coli* BL21-Codonplus (DE3)-RIL cells, and PI-PLC variants, including WT, were overexpressed and purified as described previously (36–38). Purity of PI-PLC variants was >90%, as monitored by sodium dodecyl sulfate-polyacrylamide gel electrophoresis (SDS-PAGE); protein concentrations were measured by both Lowry assays and the absorption at 280 nm. Extinction coefficients at 280 nm, calculated using the ProtParam tool (39), were $\varepsilon_{280} = 65.32\ \text{mM}^{-1}\ \text{cm}^{-1}$ for WT, the 190s loop variants, and most of the Pro variants (15) or $\varepsilon_{280} = 66.81\ \text{mM}^{-1}\ \text{cm}^{-1}$ for the Pro to Tyr variants. Formation of the disulfide bond in the double Cys variant, Asn^{226}Cys/Val^{192}Cys (N226C/V192C), was confirmed using nonreducing SDS-PAGE (data not shown). For fluorescence correlation spectroscopy (FCS) experiments, a single Cys residue, N168C, was introduced. Residue 168 is far from both the PI-PLC membrane binding region and active site, and fluorescent labeling has only minor effects on binding and activity (14,15).

Secondary structure content and thermal stability of the PI-PLC variants were measured using far-UV circular dichroism (CD) on a model No. 202 CD spectrophotometer (AVIV Biomedical, Lakewood, NJ). All of the PI-PLC variants showed similar CD spectra and the secondary structure content, analyzed with the CDNN program (40), was unaltered by any of the mutations (see Fig. S2). Thermal stabilities for all PI-PLC variants (0.05 mg/mL), measured by monitoring the ellipticity at 222 nm while increasing the sample temperature 1.0° per min (36,37), are similar to WT with melting temperatures (T_m) within 1.5°C of the T_m for WT (54 ± 1°C), except for P254G, which is slightly less stable (T_m = 51°C). Thus, any differences in activity or binding are not due to significant alterations in protein structure.

^{31}P NMR enzyme assays

Specific activities of the PI-PLC enzymes in 50 mM HEPES, 1 mM EDTA, and 0.1 mg/mL bovine serum albumin (BSA), pH 7.5 at 28°C were measured by ^{31}P NMR spectroscopy (13,14) using a model No. VNMRS 600 (Varian, Cary, NC). The amount of enzyme added into different assay systems was adjusted so that <20% product was generated in 30 min for the continuous assay and 15 min for the fixed time method. The amount of PI-PLC used was 0.1–0.25 μg/mL for mixed micelle assays, 0.2–2 μg/mL for PI cleavage when presented in vesicles, and 5–100 μg/mL for cIP hydrolysis. Cleavage rates for PI solubilized in detergent micelles and hydrolysis of cIP were measured by continuously monitoring the relative integrated intensity of the cIP or I-1-P resonance (with ^{1}H decoupling but no nuclear Overhauser effect), respectively, as a function of reaction time. The slope of this plot was used to calculate the specific activity. Mixed micelles of PI with Triton X-100 (TX-100) or diC$_7$PC were prepared by addition of the detergent solution to dry PI and were optically clear after mixing. Mixed micelles examined were either PI (8 mM)/TX-100 (16 mM) or PI (8 mM)/diC$_7$PC (32 mM). The water-soluble substrate cIP (20 mM) was used in the absence or presence of 8 mM diC$_7$PC.

For the specific activities of PI-PLC toward PI in small unilamellar vesicles (SUVs), prepared by sonication, the enzyme and SUVs were incubated for fixed times at 28°C and the reaction was quenched by addition of a few drops of acetic acid followed by TX-100 addition to solubilize the

remaining lipids in mixed micelles. The relative integrated intensity of the cIP resonance versus the total phospholipid concentration (initial [PI]+[POPC]) was used to calculate PI-PLC–specific activity. For assays of N168C PI-PLC variants acting on SUVs (see Table S1 in the Supporting Material), 5 mM dithiothreitol was added to the assay solution to avoid formation of any protein dimers.

PI-PLC SUV binding assays

PI-PLC N168C variants were fluorescently labeled with AF488 as described previously in Pu et al. (14,15). Fluorescence correlation spectroscopy (FCS)-based binding assays were performed on a lab-built confocal setup based on an IX-70 inverted microscope (Olympus, Melville, NY) (14,15). AF488 fluorescence was monitored at 22°C with samples placed in chambered coverglass wells (Lab-Tek; Nunc, Thermo Fisher Scientific, Rochester, NY), containing 10-nM labeled PI-PLC (*WT, *P(cap)X, or *P(kink)X, X = Ala or Tyr; the asterisk denotes N168C) plus 1 mg/mL BSA in 300 μL phosphate-buffered saline (PBS) buffer, pH 7.4. To prevent protein adhesion to the wells, the chambers were incubated with 10 mg/mL BSA and rinsed with PBS before use. The anionic substrate analog DOPG was used for all FCS experiments because the PI cleavage product DAG leads to vesicle fusion (41). SUVs containing DOPG and various mole fractions of POPC, expressed as the value X_{PC}, were titrated into the labeled PI-PLC solutions to assess protein binding (14,15). All of the FCS binding assays were performed in parallel with *WT binding assays for direct comparisons of apparent K_d values.

FCS experiments were performed using 488-nm excitation as described previously in Pu et al. (14,15). To account for the possibility that multiple proteins could bind to the same vesicle, autocorrelations ($G(\tau)$) (obtained in cross-correlation mode using a 50:50 beamsplitter) for samples containing SUVs were fit to (42,43)

$$G(\tau) = A_p g_p(\tau) + A_v g_v(\tau), \tag{1}$$

where p and v denote free protein and SUVs that are fluorescent due to PI-PLC binding, respectively, and A_j is the amplitude of species j. The correlation function for species j, $g_j(\tau)$ is given by (44,45)

$$g_j(\tau) = \left(1+\frac{\tau}{\tau_{D,j}}\right)^{-1}\left(1+\frac{\tau}{S^2\tau_{D,j}}\right)^{-1/2}, \tag{2}$$

$$\tau_{D,j} = \frac{\omega_o^2}{4D_j}, \tag{3}$$

$$S = \frac{z_o}{\omega_o}, \tag{4}$$

where the values of ω_o (the radius of the observation volume), and S (which depends on z_o, the extent of the observation volume), were determined from fits to rhodamine 110 calibration data using $D = 280\ \mu m^2\ s^{-1}$ at 22°C (46). The value $\tau_{D,j}$ is the diffusion time and D_j is the diffusion coefficient. The fraction of protein bound to SUVs, f, may be determined from A_p and the time-averaged number of proteins in the observation volume in the absence of vesicles, $\langle N_o\rangle$ (43):

$$f = 1 - A_p\langle N_o\rangle = \frac{1-A_p}{A_{p,o}}, \tag{5}$$

where $A_{p,o} = 1/\langle N_o\rangle$ is the amplitude for free PI-PLC before titration determined from a single species fit. When calculating f, the value $A_{p,o}$ is corrected for any volume changes from the titration. A more detailed discussion of the FCS fits may be found in Table S2 and Fig. S3, Fig. S4, and Fig. S5.

For *WT, f values determined using Eqs. 1–5 (see Fig. S4) were similar to those we determined previously (14,15) where we assumed that on average, one PI-PLC is bound per SUV. The average brightness of the SUVs relative to the protein (43), $\alpha = A_v/(A_{p,o}\text{-}A_p)$, is shown in Fig. S5 as a function of phospholipid concentration for WT PI-PLC. In low-affinity conditions, $\alpha \sim 1$ indicating that, on average, one protein is bound per vesicle. For conditions where WT PI-PLC has high affinity for vesicles, the value α is dependent on the vesicle concentrations with $\alpha \sim 1$ at low and high vesicle concentrations and $\alpha = 2$–3 for moderate vesicle concentrations, indicating that more than one protein binds to each vesicle.

The apparent dissociation constant, K_d, representing PI-PLC partitioning to the vesicle surface, and a cooperativity coefficient, n, was determined using the empirical equation (14,15)

$$f = \frac{f_{max}[PL]^n}{(K_d^n + [PL]^n)}, \tag{6}$$

where f is determined for different total lipid concentrations, [PL], at fixed X_{PC}, and f_{max} is the apparent maximum fraction bound. Representative correlation and binding curves are shown in Fig. S4. As previously noted, SUVs are quite heterogeneous, and this heterogeneity leads to f_{max} values of <100% (see Table S2 and Fig. S3) (15). For pure POPC, the binding curves have the expected hyperbolic shape, and fits were performed with n fixed to 1. However, for POPC/DOPG mixtures with $X_{PC} < 0.4$, plots of f versus [PL] are noticeably sigmoidal and n was fit. This apparent cooperativity likely results from PI-PLC's preference either for the subpopulation of vesicles with higher PC contents or for PC-rich regions in the vesicles, both of which are scarce when X_{PC} is low. For single vesicle concentrations at specific X_{PC} compositions, FCS titrations were run in duplicate and were repeated with different vesicle and protein preparations.

RESULTS

MD simulations and correlated motions

For the protein in solution, calculation of the root-mean-square fluctuations (RMSF) from the last 15 ns of the *B. cereus* PI-PLC MD simulations reveal prominent fluctuations from the equilibrium structure in regions 39–47, 123–125, 188–192, 201–203, and 238–245 (Fig. 1, *A* and *B*). PCA of the MD simulations was used to determine whether these fluctuations are associated with collective motions that could be correlated with activity and/or binding (47). In all of the WT simulations, the first and second principal components show a clamshell-like motion, with β-strands 1–5, along with associated loops and helices, apparently moving as one unit and strands 5b–8 moving as a second unit (see Movie S1 and Movie S2 in the Supporting Material). This motion is telegraphed by the pendulum-like motion of the 190s loop (residues 188–192) connecting strands 5b and 6. The clamshell-like behavior also coordinates motions of the helix B region (39–47) on one side of the clamshell and the loops N-terminal to helix F (201–203) and helix G (238–245) on the other. This collective motion, in which the loops and helix B open and close over the active site, is associated with the kinking of helix G about Pro^{254} (referred to as P(kink)). Previous work also identified helices B and G as important for PI-PLC membrane binding (15,38,48). In the TIM barrel superfamily, the loop between strand 7 and helix G is often part of a phosphate-binding

motif (6). Dynamics of this loop are also important in the activity of other TIM barrels. In triosephosphate isomerase (TIM), the corresponding loop is the active site lid (49) while motions of this same loop, containing the catalytic Cys^{319}, are important for activity and allostery in inosine monophosphate dehydrogenase (IMPDH) (50).

If the helix B, F, and G regions that close over the active site are important for enzyme activity, there might be significant sequence-conservation in these regions. Analysis of the PI-PLC MSA showed that this region is quite divergent in the PI-PLC family, consistent with the diversity of lipid-binding specificities. However, clustering the MSA using just the helix G region revealed that the phosphate-binding loop is relatively conserved in secreted PI-PLCs from extracellular bacterial pathogens and soil bacteria (Fig. 1 *D*). In these species, the Pro in helix G associated with kinking, Pro^{254}, is 100% conserved whereas the Pro that caps helix G, Pro^{245}, is less conserved. The conservation in this region as well as its association with membrane binding led us to mutate these Pro residues both in silico and in vitro. To avoid confusion between 245 and 254, we will refer to Pro^{245}X variants as P(cap)X and to Pro^{254}X variants as P(kink)X, where X is the residue at position 245 or 254 in the respective variant. We used three types of mutations:

1. Pro to Gly, which may increase flexibility and thus dynamics,
2. Pro to Ala aimed at either uncapping or unkinking helix G, and
3. Pro to Tyr mutants designed to alter phospholipid binding.

An additional Tyr residue near or in helix G, which is already rich in Tyr residues associated with membrane binding (15), should increase the probability of π-cation interactions with choline moieties in the membrane (48,51,52).

All of the Pro variants show reduced RMSFs relative to wild-type, particularly for the 190s loop (Fig. 1, *B* and *C*). For the P(cap) mutants, the anticorrelation between movements of the N-terminal two-thirds of the protein and C-terminal one-third is lost (Fig. 2, *B* and *C*). In a similar vein, the clamshell-like motion in the first two principal components is damped in P(kink)Y and essentially disappears in P(kink)A (see Fig. S6) and the loop motions over the active site appear much less coordinated in both kink variants, particularly P(kink)Y. These significant changes in the MD simulations suggested that mutating either of these Pro residues would alter *Bacillus* PI-PLC activity and/or lipid binding.

In WT, beginning with either 245 or 254 as the root residue, chained correlation analysis (24,25) reveals a large network of correlations encompassing most of the C-terminal lobe of PI-PLC (Fig. 2 *A*). The correlations found throughout this region are consistent with the observation that this comprises one of the two shells in the clamshell-like opening-closing motion found via PCA. Similar clamshell motions in the PCA, and chained correlations, are observed in MD simulations of PI-PLC bound to DMPC membranes (Fig. 2 *B*), suggesting that the clamshell motion and associated correlations may be important both in solution and on the membrane. Both the P(cap) and P(kink) mutations substantially decrease the extent of these correlations, as is most evident in the loss of chained correlations between helices F and G (Fig. 2, *C* and *D*). Whereas the exact details of the correlation maps and chained correlation vary when simulations are repeated, clamshell-like PCA and chained correlations between helices F and G are observed for all of the wild-type simulations, in the presence or absence of a membrane, and are diminished or lost in all of the P(cap) and P(kink) simulations. The effects of mutations on dynamics are also evident in cross-correlation maps calculated from the simulations.

In WT, the clamshell-like motion is most clearly evident from the fact that residues 40–50 and 120–125 show significant anticorrelation with residues ~170–200, 230–250, and 265–275 (*rectangular regions*, Fig. 2 *A*). These anticorrelations reflect helix B and the loop connecting strand 3 and helix E moving in opposition to the canonical TIM barrel phosphate-binding loop, the tyrosine strip at the top of helix G, the 190s loop, and strand 8. These strong anticorrelations are largely absent in both the Tyr and Ala mutants. Such anticorrelated breathing motions are also not observed in MD simulations for *L. monocytogenes* PI-PLC (23) (which also lacks chained correlations between helices F and G (see Fig. S7)). Unlike *Bacillus, Listeria* is an intracellular pathogen, and *L. monocytogenes* PI-PLC displays very low activity toward GPI-anchored proteins (53); its enzymatic activity is not enhanced by specific interactions with PC, although many amphiphiles can enhance its activity (54). *Listeria* and *Bacillus* PI-PLCs thus exhibit differences in dynamics, lipid, and substrate specificity, suggesting that altering *Bacillus* PI-PLC dynamics could affect enzyme specificity.

Phosphotransferase activity in micelles

PI dispersed in diC_7PC micelles is a better PI-PLC phosphotransferase substrate than PI presented in TX-100 micelles (11,13) and the same trend is observed for the Pro variants. The P(cap) variants all show decreased activity toward PI/TX-100 mixed micelles, with P(cap)A retaining the most activity (Fig. 3 *A*). When PI is solubilized in diC_7PC micelles, enzymatic activity is enhanced, but the cap variants still exhibit lower activity than WT.

The kink variants exhibit a very different profile with the mixed micelles. For PI/TX-100, P(kink)A was significantly more active than WT (993 ± 168 vs. 621 ± 151 μmol min^{-1} mg^{-1}) although P(kink)G and P(kink)Y have lower activity than WT. For PI in diC_7PC micelles, activities of the kink variants are equivalent to WT. Combining the Ala

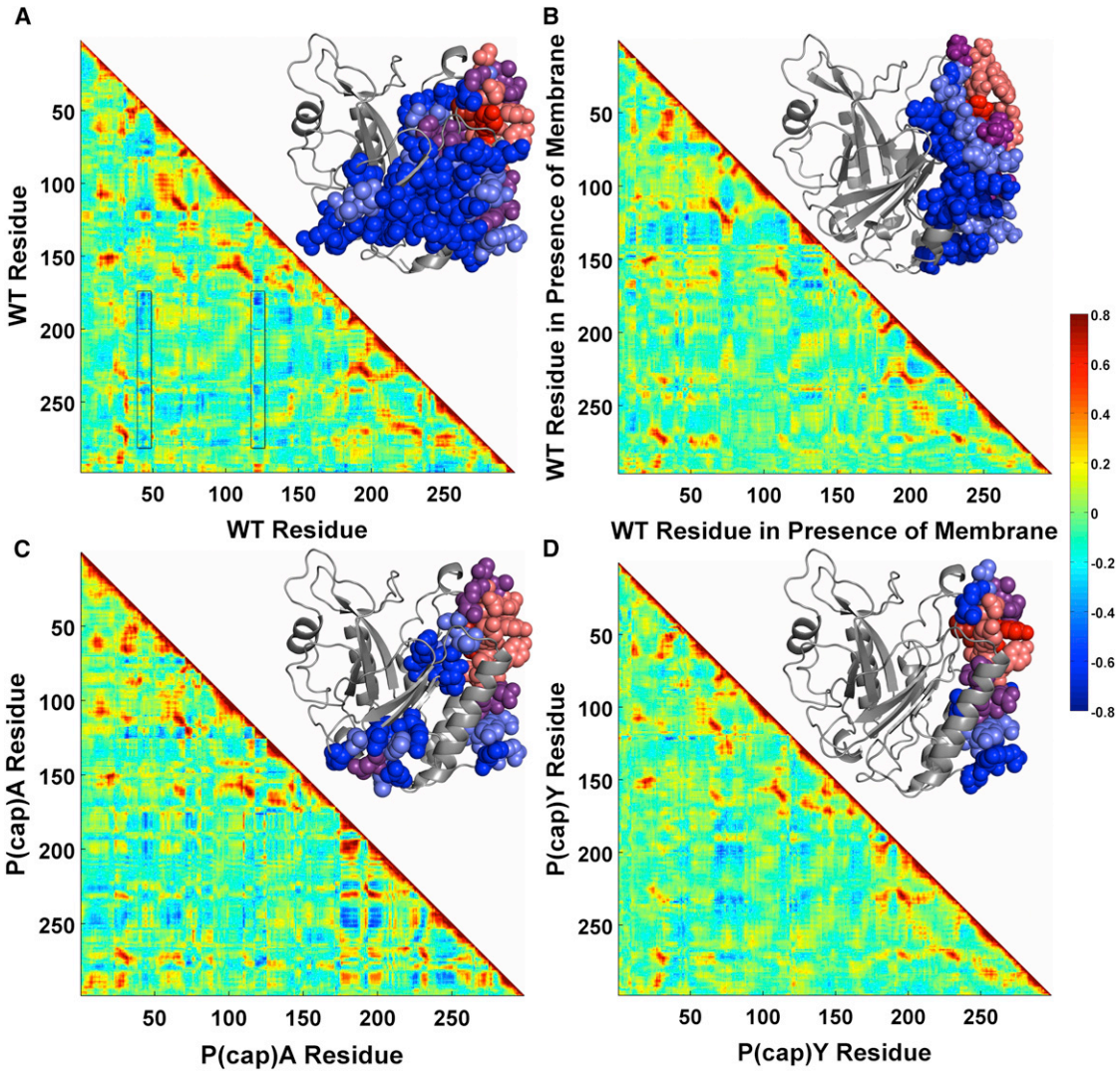

FIGURE 2 Replacement of the cap Pro residue disrupts correlated motions in the PI-PLC MD simulations. Cross-correlation maps and chained correlations for (*A*) WT, (*B*) WT in the presence of a DMPC membrane, (*C*) P(cap)A, and (*D*) P(cap)Y PI-PLC. The color-scale for the correlation maps goes from anticorrelated motions (*dark blue*) to correlated motions (*red*). The results from the chained correlation calculation are superimposed on the protein structure with residues participating in chained correlations with position 245 (P(cap)) shown as spheres colored according to iteration number (see text): (*red spheres*) first iteration to (*blue spheres*) last iteration. The rectangular areas in the WT correlation map highlight the anticorrelated motions.

mutations, P(cap)A/P(kink)A, results in a variant with ~50% of the P(cap)A activity toward PI in both TX100 and diC_7PC micelles despite the benign effects of the P(kink)A mutation.

Phosphodiesterase activity with and without micelles

The second step in the PI-PLC reaction, cIP hydrolysis to I-1-P, can be mimicked by incubating soluble cIP with PI-PLC. Although the enzyme, substrate, and product in this reaction are all soluble, addition of PC micelles greatly enhances activity (Fig. 3 *B*) (13). For the cap variants, changes in cIP cleavage rates are complex. In the absence of diC_7PC, P(cap)A and P(cap)G displayed 50% and ~10% of the WT specific activity, respectively. In contrast, the specific activity of P(cap)Y was approximately twofold higher than WT. This higher activity may reflect improved cIP binding, which is quite weak for WT (48). In many proteins that bind a myo-inositol moiety, including PI-PLC, a tyrosine is seen to stack with the inositol ring and its removal destabilizes binding (4,5). Placing a Tyr in the cap position may aid in positioning cIP in the active site. Addition of diC_7PC increased the activity for all of the cap variants, but the activities were still far below WT. For the kink variants, specific activities were at least 50% of WT and the cIP hydrolysis rate with micellar diC_7PC present increased 24 $\pm$ 2 times similar to that observed for WT PI-PLC. The double Pro variant, P(cap)A/P(kink)A, behaved similarly to P(cap)A, suggesting that the cap

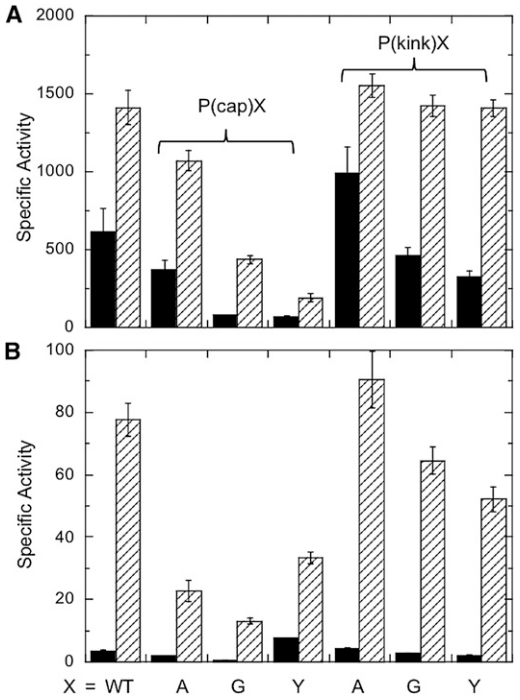

FIGURE 3 Specific activities (μmol min^{-1} mg^{-1}) of PI-PLC variants toward (*A*) PI solubilized in micelles and (*B*) the soluble substrate cIP. (*A*) Specific activity for PI cleavage in mixed micelles containing 8 mM PI in 16 mM TX-100 (*solid bars*) or in 32 mM diC_7PC (*hatched bars*); (*B*) Specific activity for cleavage of 20 mM cIP in the absence (*solid bars*) and presence (*hatched bars*) of 8 mM diC_7PC. The error bars are the standard deviations of the specific activities.

mutation overrides the increase in activity toward cIP observed for the P(kink)A variant.

For both types of micelle-based assays, the cap variants show greater reductions in activity than the kink variants. The cIP hydrolysis results for P(cap)A/P(kink)A suggest that the cap is key for activity toward the soluble substrate. Cap mutations also significantly reduce the activity enhancement observed in the presence of PC, suggesting that the cap plays an important role in enhancement of PI-PLC enzymatic activity by PC, perhaps related to the barrel-breathing motions observed in the WT simulation that disappear in the simulations for the cap variants.

Binding and phosphotransferase activity for vesicles

PI-PLC partitioning to vesicles is inextricably linked to activity, and PC content significantly enhances binding. PI-PLC prefers SUVs to the less curved large unilamellar vesicles (14), and WT PI-PLC has an apparent K_d of 4–6 mM for pure PG SUVs in PBS buffer. Addition of PC leads to substantial drops in K_d for $X_{PC} = 0.1$–0.5 and increases in enzymatic activity. The extent of the activity increase is dependent on the PI concentration with respect to K_d. For 8–10 mM PI, i.e., concentrations considerably above the apparent K_d, there is a 2–3-fold increase in specific activity with the addition of PC suggesting that this nonsubstrate phospholipid activates the enzyme by more than just anchoring the protein to the vesicle (14,15). However, whereas the apparent K_d continues to drop, reaching a minimum of ~1 μM at $X_{PC} = 0.8$, activity is greatly reduced for $X_{PC} > 0.5$. Very tight binding sequesters the enzyme on the vesicle surface, apparently in PC-rich regions, leading to reduced activity (14).

How are SUV activity and binding related for the Pro variants?

Despite its reduced activity in the micelle assays, the apparent K_d of P(cap)A for SUVs is virtually identical to that of WT for pure PG SUVs and only 2–3 times higher than WT in the presence of PC (Fig. 4 *A*). Specific activities of P(cap)A toward PI/PC SUVs were almost the same as WT across the X_{PC} range examined (Fig. 4 *B*). In contrast to the Ala variant, the P(cap)Y variant binds much less tightly to SUVs, with apparent K_d values between 0.5 and 0.9 X_{PC} that are more than an order-of-magnitude higher than WT (Fig. 4 *A*). This loss of binding affinity is associated with reduced activity of P(cap)Y for PI in SUVs,

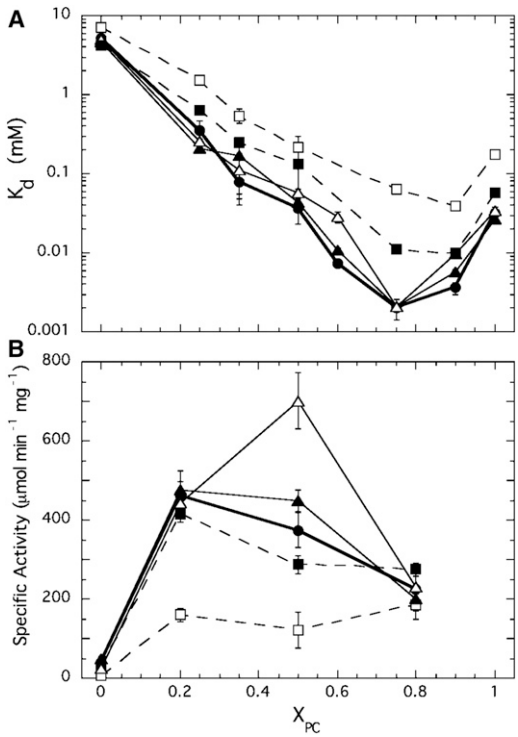

FIGURE 4 Membrane binding and activity toward SUVs. (*A*) PI-PLC binding to DOPG/POPC SUVs as a function of the mole fraction PC, X_{PC}. (*B*) Variation of the specific activity of PI-PLC Pro variants toward PI/POPC SUVs with 8 mM PI and varying X_{PC}: WT (●), P(cap)A (■), P(cap)Y (□), P(kink)A (▲), and P(kink)Y (△). The error bars are the standard errors determined from two independent protein and SUV preparations.

although the concentration of substrate in SUVs was well above the apparent K_d values. However, what is striking for P(cap)Y is that the specific activity does not drop at $X_{PC} = 0.8$ where WT activity drops ~50%, in part because of sequestration of the enzyme in PC-rich regions (14). Instead, the specific activity of P(cap)Y is constant in the range of $X_{PC} = 0.2$–0.8. Lower affinity for SUVs may be an advantage at high X_{PC}, allowing the enzyme to access the next substrate lipid (15).

The kink variants behave quite differently (Fig. 4). P(kink)A is relatively nonperturbing with binding affinities and activities that are similar to WT. P(kink)Y binding affinities are similar to WT except for $X_{PC} = 0.5$–0.6 where the apparent K_d values are 2–3 times higher. These differences in K_d would not be noteworthy, except for the anomalous activity of P(kink)Y toward both pure PI SUVs, where its activity is only 60% that of WT despite nearly identical apparent K_d values, and its activity toward SUVs with $X_{PC} = 0.5$ (1:1 PI/PC) where it, reproducibly, has 1.9-times WT-specific activity. This increase in activity is not readily explained by its slightly lower affinity for SUVs. The lower specific activity of P(kink)Y in the absence of PC for both pure PI SUVs and cIP, as well as the generally reduced activity of P(kink)Y despite lipid binding affinities that are similar to WT, suggest that freezing PI-PLC motions are particularly detrimental for activity.

Restricting dynamics of the 190s loop

Although the simulations suggest that mutating the Pro residues in helix G alter dynamics, thus affecting enzymatic activity and binding as discussed above, crosslinking the loops involved in the clamshell-like motions would provide a more direct test of the relationship between dynamics and activity. Unfortunately, many of the structural elements that contribute to the lowest frequency modes are known to be crucial for binding and activity, e.g., helix B and the phosphate-binding loop. We therefore chose to alter the dynamics of the 190s loop on the other side of PI-PLC, a region of the protein not previously associated with enzymatic activity or binding because it is far from both the active site and the lipid-binding regions containing helices B, F, and G and associated loops (Fig. 1 *A*). Nonetheless, obvious, pendulum-like motions of this loop are correlated with the motions in the helix B, F, and G regions (see Movie S1 and Movie S2), and constraining this loop should alter PI-PLC dynamics. Two sets of mutations were designed to alter 190s loop motions:

1. The loop was constrained in the V192C/N226C construct by introducing a disulfide bond between the 190s loop and an adjacent loop.
2. The flexibility of the 190s loop was altered by introducing a Pro residue between Gln^{190} and Asn^{191} (Q190-P-N191).

Despite the distance of this loop from the PI-PLC active site and membrane-binding regions, both variants display <40% of the wild-type activity toward pure PI SUVs (Fig. 5), which is a lower activity than all of the helix G Pro variants except for P(cap)Y (which has only 15% of the WT activity). The activity deficits of the 190s loop variants are rescued at 0.2 X_{PC}, whereas at 0.8 X_{PC} the disulfide-bonded variant has slightly more activity than WT and Q190-P-N191 displays 70% of the WT activity. The activity trend for the 190s loop variants resembles those of the helix G Pro-to-Ala variants, suggesting that these very different sets of mutations may have similar effects on PI-PLC dynamics and activity.

DISCUSSION

Experimentally measuring changes in dynamics is particularly difficult for peripheral membrane proteins such as PI-PLC that dynamically associate and dissociate from the interface. For these enzymes, catalysis requires two discrete steps—the initial partitioning of the protein to the bilayer surface, followed by docking of a substrate into the active site in the optimal orientation. MD simulations provide a way to predict how mutations may alter the dynamics of the free protein conformation that first interacts with the membrane and the effects of interesting mutations on protein partitioning and/or activity can then be determined experimentally. Naively, one might expect that alterations in the free protein dynamics would compromise binding but have little effect on the activity of the membrane-bound enzyme. However, for PI-PLC variants that are predicted to have altered dynamics, activity is more likely to be perturbed than binding. While partitioning to the membrane likely alters the conformation and/or dynamics of the mobile loops and helices that contact the interface, much of the protein is not in contact with the surface and some of the lowest energy modes may still be accessible, as observed for the MD simulations performed in the presence

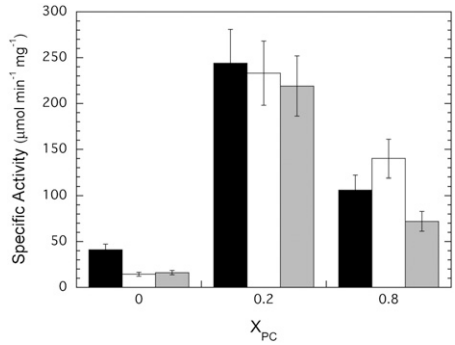

FIGURE 5 Constraining the 190s loop lowers activity toward pure PI SUVs. Specific activities of the 190s loop variants toward SUVs with increasing PC content: WT (*black*), V192C/N226C (*white*), and Q190-P-N191 (*gray*).

of a membrane (Fig. 2 *B*). Constraints on the conformation and dynamics of the bound protein may also be different between SUVs and the even more highly curved micelles.

The relative conservation of the putative PC binding regions in extracellular bacterial pathogens, the likely importance of this region in membrane binding and the correlated loop motions observed in the MD simulations focused our attention on the helix B and G regions. Helix G is a long helix containing several Tyr residues known to be important for interfacial binding (38,48). Pro mutations in this helix do disrupt the correlated motions observed in the simulations. P(cap) (Pro^{245}), the Pro cap for helix G, is >9 Å from the active site and could directly interact with substrate as it enters the active site in addition to directly affecting membrane binding as well as protein conformation and dynamics. In contrast, P(kink) (Pro^{254}), the Pro in the middle of helix G around which the helix kinks in the MD simulations, is >15 Å distance from the active site, and both this distance and its location in the helix preclude direct interactions with substrates. Since no significant effects on binding are observed for the P(kink) variants, changes in activity are likely due to altered protein conformations or dynamics.

Despite similarities in how the Pro mutations reduce the RMSF of loops in the MD simulations (Fig. 1), the P(cap) variants generally have larger effects on PI-PLC activity and binding than do the P(kink) variants. The Pro cap is N-terminal to Tyr residues 246–248 that are important for binding to membranes containing PC (15,48). Mutagenesis of all three of these Tyr residues to Ser results in low binding affinity for and activity toward SUVs containing PC (15). Interestingly, of the cap variants, P(cap)Y, which might have been expected to aid in π-choline cation interactions with PC, exhibits the lowest affinity for PC-rich SUVs. The loss in activity of the P(cap) variants is also observed for micelle-based assays and activity toward the soluble substrate cIP. Removing Pro^{245} likely alters the accessible conformations near the N-terminus of helix G, reducing the probability that the Tyr residues bind to the membrane. Alternatively, the alterations in dynamics observed in the P(cap) variant MD simulations could also reduce the active-site binding affinity for substrate.

While in silico mutagenesis of P(kink) (Pro^{254}, the Pro about which helix G flexes) has large effects on the MD simulations (i.e., damping the fluctuations throughout the protein), the P(kink) variants show much smaller deficits in activity and binding. In the P(kink)A MD simulations, the extended rather than kinked helix G freezes motions in a manner that leaves the active site open. This dynamical change would favor substrate access to the active site, resulting in little change in activity or overall vesicle binding, as observed experimentally. In WT, helix B as well as the helix F and G loops close and open over the active site in a coordinated manner; however, loop motion is uncoordinated in P(kink)Y, and in the first principal component occlusion of the active site appears more likely. This would translate to the observed lower specific activity of P(kink)Y in the absence of PC (where only active-site binding occurs). In the presence of PC, the helix G region, which has been implicated in binding PC, would be more constrained, presumably favoring an open active site. This analysis argues that enhancement of activity by PC results because PC binding constrains both the helix G and the helix B regions, which would otherwise intermittently limit access to the active site. This picture is supported by mutations in the 190s loop designed to restrict dynamics. For these variants, decreases in activity are largest in the absence of PC, and rescued by low mol % PC, again suggesting that PC binding serves to constrain loops and helices enhancing access to the active site.

For both the P(kink) and P(cap) variants, changes in activity are not consistently correlated with changes in binding. The P(kink) variants bind to vesicles with apparent K_d values that are similar to wild-type despite changes in activity, whereas defects in P(cap)Y activity appear to be larger than would be predicted from the increase in apparent K_d. However, in all cases, changes in activity appear to be correlated with the changes in enzyme dynamics observed in the free protein simulations. Many studies of both all-atom and coarse-grained protein models have found that the lowest frequency motions, such as those identified from the first few principal components in PCA, are often intrinsic to the protein structure and independent of the membrane environment (55). This finding is supported by the results from the protein-plus-membrane simulations where the clamshell-like movements of the PI-PLC β-barrel are largely unaffected by membrane binding. Thus, despite the constraints imposed by interfacial binding, the dynamics and lowest energy modes of free PI-PLC in solution are likely still relevant for the membrane-bound protein.

CONCLUSIONS

The combination of MD simulations, in silico and in vitro mutagenesis along with binding and activity assays, provides a role for loop and helix motions in regulating the activity of *Bacillus* PI-PLC. In this model, the coordinated closing of the helix B region and helix G region in the free enzyme limits access to the active site, whereas PC binding in the region of helix G leads to an open active site. Structural alignments of the *Bacillus* PI-PLC (4) with the well-studied yeast TIM (56,57), as well as parasite IMPDHs (58,59), show that the phosphate-binding loop N-terminal to helix G in PI-PLC aligns with the active site lid in yeast TIM and the dynamic loop containing catalytic Cys^{319} in IMPDH from two parasites, *Tritrichomonas fetus* and *Cryptosporidium parvum*. Interestingly, while the helix C-terminal to these loops is capped by a Pro residue in yeast TIM, Pro in this position is only slightly conserved in TIM (60,61). The corresponding helix is capped by Pro in

C. parvum IMPDH but not *T. fetus* IMPDH. This is reminiscent of extracellular bacterial PI-PLCs where helix G is capped by Pro^{245} in *Bacillus* PI-PLC but not in PI-PLC from *S. aureus* (Fig. 1 *D*). A recent x-ray crystal structure of *S. aureus* PI-PLC reveals that motions of the phosphate-binding loop are mediated by a pH-dependent π-cation latch between Phe^{249} in the loop (corresponding to *Bacillus* Trp^{242}) and His^{258} in helix G (corresponding to *Bacillus* Tyr^{251}) (62). Thus, there are many ways to control the motions of this loop and associated allostery in TIM barrels, including a balance of loop rigidity and flexibility in TIM (63), ion binding in parasite IMPDH (50), and the π-cation latch in *Staphylococcus* PI-PLC. The Pro cap on helix G may be one more nonconserved way to modulate loop motions and allostery in TIM barrels.

SUPPORTING MATERIAL

Supplemental methods, two tables, seven figures, two movies, and references (65–68) are available at http://www.biophysj.org/biophysj/supplemental/S0006-3495(12)01236-2.

C.G. Parallab (the High Performance Computing Laboratory at the University of Bergen) and NOTUR, the Norwegian Metacenter for Computational Science, are gratefully acknowledged for provision of CPU time to this project. We thank Robert G. Smock for assistance with the sequence alignments.

Research reported in this publication was supported by the National Institute of General Medical Science, at the National Institutes of Health, under award No. R01GM060418 (to M.F.R.). This work was also supported by a grant from the Bergen Research Foundation (to N.R.).

REFERENCES

1. Daugherty, S., and M. G. Low. 1993. Cloning, expression, and mutagenesis of phosphatidylinositol-specific phospholipase C from *Staphylococcus aureus*: a potential staphylococcal virulence factor. *Infect. Immun.* 61:5078–5089.
2. Heffernan, B. J., B. Thomason, …, P. Hanna. 2006. *Bacillus anthracis* phospholipases C facilitate macrophage-associated growth and contribute to virulence in a murine model of inhalation anthrax. *Infect. Immun.* 74:3756–3764.
3. Mengaud, J., C. Braun-Breton, and P. Cossart. 1991. Identification of phosphatidylinositol-specific phospholipase C activity in *Listeria monocytogenes*: a novel type of virulence factor? *Mol. Microbiol.* 5:367–372.
4. Heinz, D. W., M. Ryan, …, O. H. Griffith. 1995. Crystal structure of the phosphatidylinositol-specific phospholipase C from *Bacillus cereus* in complex with myo-inositol. *EMBO J.* 14:3855–3863.
5. Moser, J., B. Gerstel, …, D. W. Heinz. 1997. Crystal structure of the phosphatidylinositol-specific phospholipase C from the human pathogen *Listeria monocytogenes*. *J. Mol. Biol.* 273:269–282.
6. Nagano, N., C. A. Orengo, and J. M. Thornton. 2002. One fold with many functions: the evolutionary relationships between TIM barrel families based on their sequences, structures and functions. *J. Mol. Biol.* 321:741–765.
7. Ikezawa, H., M. Yamanegi, …, T. Ohyabu. 1976. Studies on phosphatidylinositol phosphodiesterase (phospholipase C type) of *Bacillus cereus*. I. Purification, properties and phosphatase-releasing activity. *Biochim. Biophys. Acta.* 450:154–164.
8. Lehto, M. T., and F. J. Sharom. 2002. PI-specific phospholipase C cleavage of a reconstituted GPI-anchored protein: modulation by the lipid bilayer. *Biochemistry.* 41:1398–1408.
9. Volwerk, J. J., J. A. Koke, …, O. H. Griffith. 1989. Functional characteristics of phosphatidylinositol-specific phospholipases C from *Bacillus cereus* and *Bacillus thuringiensis*. *FEMS Microbiol. Lett.* 52:237–241.
10. Bunney, T. D., and M. Katan. 2011. PLC regulation: emerging pictures for molecular mechanisms. *Trends Biochem. Sci.* 36:88–96.
11. Zhou, C., X. Qian, and M. F. Roberts. 1997. Allosteric activation of phosphatidylinositol-specific phospholipase C: specific phospholipid binding anchors the enzyme to the interface. *Biochemistry.* 36: 10089–10097.
12. Zhou, C., and M. F. Roberts. 1998. Nonessential activation and competitive inhibition of bacterial phosphatidylinositol-specific phospholipase C by short-chain phospholipids and analogues. *Biochemistry.* 37:16430–16439.
13. Zhou, C., Y. Wu, and M. F. Roberts. 1997. Activation of phosphatidylinositol-specific phospholipase C toward inositol 1,2-(cyclic)-phosphate. *Biochemistry.* 36:347–355.
14. Pu, M., X. Fang, …, M. F. Roberts. 2009. Correlation of vesicle binding and phospholipid dynamics with phospholipase C activity: insights into phosphatidylcholine activation and surface dilution inhibition. *J. Biol. Chem.* 284:16099–16107.
15. Pu, M., M. F. Roberts, and A. Gershenson. 2009. Fluorescence correlation spectroscopy of phosphatidylinositol-specific phospholipase C monitors the interplay of substrate and activator lipid binding. *Biochemistry.* 48:6835–6845.
16. Phillips, J. C., R. Braun, …, K. Schulten. 2005. Scalable molecular dynamics with NAMD. *J. Comput. Chem.* 26:1781–1802.
17. MacKerell, A. D., D. Bashford, …, M. Karplus. 1998. All-atom empirical potential for molecular modeling and dynamics studies of proteins. *J. Phys. Chem. B.* 102:3586–3616.
18. Buck, M., S. Bouguet-Bonnet, …, A. D. MacKerell, Jr. 2006. Importance of the CMAP correction to the CHARMM22 protein force field: dynamics of hen lysozyme. *Biophys. J.* 90:L36–L38.
19. MacKerell, Jr., A. D. 2004. Empirical force fields for biological macromolecules: overview and issues. *J. Comput. Chem.* 25:1584–1604.
20. Jorgensen, W. L., J. Chandrasekhar, …, M. L. Klein. 1983. Comparison of simple potential functions for simulating liquid water. *J. Chem. Phys.* 79:926–935.
21. Olsson, M. H. M., C. R. Søndergaard, …, J. H. Jensen. 2011. PROPKA3: consistent treatment of internal and surface residues in empirical pK_a predictions. *J. Chem. Theory Comput.* 7:525–537.
22. Seeber, M., M. Cecchini, …, A. Caflisch. 2007. WORDOM: a program for efficient analysis of molecular dynamics simulations. *Bioinformatics.* 23:2625–2627.
23. Meyer, T., M. D'Abramo, …, M. Orozco. 2010. MoDEL (Molecular Dynamics Extended Library): a database of atomistic molecular dynamics trajectories. *Structure.* 18:1399–1409.
24. Camps, J., O. Carrillo, …, M. Orozco. 2009. FlexServ: an integrated tool for the analysis of protein flexibility. *Bioinformatics.* 25:1709–1710.
25. Papaleo, E., G. Renzetti, and M. Tiberti. 2012. Mechanisms of intramolecular communication in a hyperthermophilic acylaminoacyl peptidase: a molecular dynamics investigation. *PLoS ONE.* 7:e35686.
26. Klauda, J. B., R. M. Venable, …, R. W. Pastor. 2010. Update of the CHARMM all-atom additive force field for lipids: validation on six lipid types. *J. Phys. Chem. B.* 114:7830–7843.
27. Lazaridis, T. 2005. Implicit solvent simulations of peptide interactions with anionic lipid membranes. *Proteins.* 58:518–527.
28. Hajjar, E., M. Mihajlovic, …, N. Reuter. 2008. Computational prediction of the binding site of proteinase 3 to the plasma membrane. *Proteins.* 71:1655–1669.

29. Broemstrup, T., and N. Reuter. 2010. Molecular dynamics simulations of mixed acidic/zwitterionic phospholipid bilayers. *Biophys. J.* 99: 825–833.

30. Altschul, S. F., T. L. Madden, …, D. J. Lipman. 1997. Gapped BLAST and PSI-BLAST: a new generation of protein database search programs. *Nucleic Acids Res.* 25:3389–3402.

31. Papadopoulos, J. S., and R. Agarwala. 2007. COBALT: constraint-based alignment tool for multiple protein sequences. *Bioinformatics.* 23:1073–1079.

32. Marcelino, A. M. C., R. G. Smock, and L. M. Gierasch. 2006. Evolutionary coupling of structural and functional sequence information in the intracellular lipid-binding protein family. *Proteins.* 63:373–384.

33. Eisen, M. B., P. T. Spellman, …, D. Botstein. 1998. Cluster analysis and display of genome-wide expression patterns. *Proc. Natl. Acad. Sci. USA.* 95:14863–14868.

34. Saldanha, A. J. 2004. Java TREEVIEW—extensible visualization of microarray data. *Bioinformatics.* 20:3246–3248.

35. Waterhouse, A. M., J. B. Procter, …, G. J. Barton. 2009. JALVIEW Ver. 2—a multiple sequence alignment editor and analysis workbench. *Bioinformatics.* 25:1189–1191.

36. Feng, J., H. Wehbi, and M. F. Roberts. 2002. Role of tryptophan residues in interfacial binding of phosphatidylinositol-specific phospholipase C. *J. Biol. Chem.* 277:19867–19875.

37. Guo, S., X. Zhang, …, M. F. Roberts. 2008. Role of helix B residues in interfacial activation of a bacterial phosphatidylinositol-specific phospholipase C. *Biochemistry.* 47:4201–4210.

38. Shi, X., C. Shao, …, M. F. Roberts. 2009. Modulation of *Bacillus thuringiensis* phosphatidylinositol-specific phospholipase C activity by mutations in the putative dimerization interface. *J. Biol. Chem.* 284:15607–15618.

39. Gasteiger, E., C. Hoogland, …, A. Bairoch. 2005. Protein identification and analysis tools on the ExPASy server. *In* Proteomics Protocols Handbook. J. M. Walker, editor. Humana Press, New York. 571–607.

40. Böhm, G., R. Muhr, and R. Jaenicke. 1992. Quantitative analysis of protein far UV circular dichroism spectra by neural networks. *Protein Eng.* 5:191–195.

41. Goñi, F. M., and A. Alonso. 2000. Membrane fusion induced by phospholipase C and sphingomyelinases. *Biosci. Rep.* 20:443–463.

42. Middleton, E. R., and E. Rhoades. 2010. Effects of curvature and composition on α-synuclein binding to lipid vesicles. *Biophys. J.* 99:2279–2288.

43. Rusu, L., A. Gambhir, …, J. Rädler. 2004. Fluorescence correlation spectroscopy studies of peptide and protein binding to phospholipid vesicles. *Biophys. J.* 87:1044–1053.

44. Elson, E. L., and D. Magde. 1974. Fluorescence correlation spectroscopy. I. Conceptual basis and theory. *Biopolymers.* 13:1–27.

45. Thompson, N. L. 1991. Fluorescence correlation spectroscopy. *In* Topics in Fluorescence Spectroscopy. J. R. Lakowicz, editor. Plenum Press, New York. 337–378.

46. Magde, D., E. L. Elson, and W. W. Webb. 1974. Fluorescence correlation spectroscopy. II. An experimental realization. *Biopolymers.* 13:29–61.

47. Kitao, A., and N. Go. 1999. Investigating protein dynamics in collective coordinate space. *Curr. Opin. Struct. Biol.* 9:164–169.

48. Pu, M., A. Orr, …, M. F. Roberts. 2010. Defining specific lipid binding sites for a peripheral membrane protein in situ using subTesla field-cycling NMR. *J. Biol. Chem.* 285:26916–26922.

49. Joseph, D., G. A. Petsko, and M. Karplus. 1990. Anatomy of a conformational change: hinged "lid" motion of the triosephosphate isomerase loop. *Science.* 249:1425–1428.

50. Riera, T. V., L. Zheng, …, L. Hedstrom. 2011. Allosteric activation via kinetic control: potassium accelerates a conformational change in IMP dehydrogenase. *Biochemistry.* 50:8508–8518.

51. Ma, J. C., and D. A. Dougherty. 1997. The cation-π interaction. *Chem. Rev.* 97:1303–1324.

52. Sanderson, J. M., and E. J. Whelan. 2004. Characterization of the interactions of aromatic amino acids with diacetyl phosphatidylcholine. *Phys. Chem. Chem. Phys.* 6:1012–1017.

53. Goldfine, H., and C. Knob. 1992. Purification and characterization of *Listeria monocytogenes* phosphatidylinositol-specific phospholipase C. *Infect. Immun.* 60:4059–4067.

54. Chen, W., H. Goldfine, …, M. F. Roberts. 2009. *Listeria monocytogenes* phosphatidylinositol-specific phospholipase C: kinetic activation and homing in on different interfaces. *Biochemistry.* 48:3578–3592.

55. Bahar, I., T. R. Lezon, …, I. H. Shrivastava. 2010. Normal mode analysis of biomolecular structures: functional mechanisms of membrane proteins. *Chem. Rev.* 110:1463–1497.

56. Davenport, R. C., P. A. Bash, …, D. Ringe. 1991. Structure of the triosephosphate isomerase-phosphoglycolohydroxamate complex: an analogue of the intermediate on the reaction pathway. *Biochemistry.* 30:5821–5826.

57. Lolis, E., T. Alber, …, G. A. Petsko. 1990. Structure of yeast triosephosphate isomerase at 1.9-Å resolution. *Biochemistry.* 29:6609–6618.

58. MacPherson, I. S., S. Kirubakaran, …, L. Hedstrom. 2010. The structural basis of *Cryptosporidium*-specific IMP dehydrogenase inhibitor selectivity. *J. Am. Chem. Soc.* 132:1230–1231.

59. Prosise, G. L., and H. Luecke. 2003. Crystal structures of *Tritrichomonas fetus* inosine monophosphate dehydrogenase in complex with substrate, cofactor and analogs: a structural basis for the random-in ordered-out kinetic mechanism. *J. Mol. Biol.* 326:517–527.

60. Sun, J., and N. S. Sampson. 1998. Determination of the amino acid requirements for a protein hinge in triosephosphate isomerase. *Protein Sci.* 7:1495–1505.

61. Xiang, J., J. Sun, and N. S. Sampson. 2001. The importance of hinge sequence for loop function and catalytic activity in the reaction catalyzed by triosephosphate isomerase. *J. Mol. Biol.* 307:1103–1112.

62. Goldstein, R., J. Cheng, …, M. F. Roberts. 2012. Structure of the *S. aureus* PI-specific phospholipase C reveals modulation of active site access by a titratable π-cation latched loop. *Biochemistry.* 51:2579–2587.

63. Kempf, J. G., J. Y. Jung, …, J. P. Loria. 2007. Dynamic requirements for a functional protein hinge. *J. Mol. Biol.* 368:131–149.

64. Pettersen, E. F., T. D. Goddard, …, T. E. Ferrin. 2004. UCSF CHIMERA—a visualization system for exploratory research and analysis. *J. Comput. Chem.* 25:1605–1612.

65. Feller, S. E., Y. Zhang, …, B. R. Brooks. 1995. Constant pressure molecular dynamics simulation: the Langevin piston method. *J. Chem. Phys.* 103:4613–4621.

66. Izaguirre, J. A., S. Reich, and R. D. Skeel. 1999. Longer time steps for molecular dynamics. *J. Chem. Phys.* 110:9853–9864.

67. Essmann, U., L. Perera, …, L. G. Pedersen. 1995. A smooth particle mesh Ewald method. *J. Chem. Phys.* 103:8577–8593.

68. Andersen, H. C. 1983. RATTLE: a "velocity" version of the SHAKE algorithm for molecular dynamics calculations. *J. Comput. Phys.* 52:24–34.